Nonlinear resonant coupling between two adjacent bays

Marta Marcos[1]
Cross-Disciplinary Oceanographic Group/Physical Oceanography (GOIFs), IMEDEA (CSIC-UIB), Esporles, Mallorca, Spain

Philip L.-F. Liu
School of Civil and Environmental Engineering, Cornell University, Ithaca, New York, USA

Sebastià Monserrat[1]
Cross-Disciplinary Oceanographic Group/Physical Oceanography (GOIFs), IMEDEA (CSIC-UIB), Esporles, Mallorca, Spain

Received 9 July 2003; revised 18 February 2004; accepted 24 February 2004; published 5 May 2004.

[1] Field evidences of the nonlinear resonant coupling between two adjacent basins are found in two elongated inlets in the region of Ciutadella, Menorca Island, in the western Mediterranean. Sea level measurements reveal different amplification responses during calm periods (when a linear approach is justified) and during "rissaga" events (when sea level oscillations inside the bays reach amplitudes comparable to water depth and nonlinear effects are expected to play a significant role). These differences are then interpreted as the observational manifestation of the nonlinear coupling between two adjacent inlets. This phenomenon is studied using a simplified analytical model consisting of two parallel and rectangular adjacent inlets with constant depth. Weakly nonlinear and weakly dispersive waves are considered. Therefore Boussinesq equations may be employed for the analysis. The problem is further simplified by assuming that the waves outside the bays are linear so that the wave fields inside the bays can be described by a system of coupled nonlinear two-point boundary value problems with complex coefficients for each harmonic. The nonlinear system is solved numerically, and the solutions are used to investigate the coupling under linear and nonlinear wave conditions. *INDEX TERMS:* 4546 Oceanography: Physical: Nearshore processes; 4203 Oceanography: General: Analytical modeling; 4560 Oceanography: Physical: Surface waves and tides (1255); 4219 Oceanography: General: Continental shelf processes; 4564 Oceanography: Physical: Tsunamis and storm surges; *KEYWORDS:* nonlinear coupling, Boussinesq equations, western Mediterranean

Citation: Marcos, M., P. L.-F. Liu, and S. Monserrat (2004), Nonlinear resonant coupling between two adjacent bays, *J. Geophys. Res.*, *109*, C05008, doi:10.1029/2003JC002039.

1. Introduction

[2] Harbor resonance occurs when one of the natural modes of the harbor is excited by a forcing mechanism, including underwater earthquakes, landslides, atmospheric pressure disturbances and infragravity waves. Large amplitude wave motions inside a harbor during a resonance event could cause severe damages to moored vessels and impair marine operations. For these important practical reasons, many research works have been performed to improve our understanding of the fundamental features of harbor resonance [*Miles*, 1994]. Most of these research works are based on linear wave theories and corresponding numerical models have also been developed for analyzing wave oscillations inside a harbor with complex geometry [*Panchang and Demirbilek*, 2001]. Solutions based on a linear wave theory are very useful in determining the natural modes of a given harbor configuration and in estimating the magnitude of harbor responses. Obviously, linear wave theories break down near the resonance frequencies, where the wave amplitudes could increase by an order of magnitude.

[3] To investigate the nonlinear effects on harbor oscillations, *Rogers and Mei* [1978] (hereinafter referred to as R&M) proposed a matched asymptotic method to obtain numerical solutions for wave oscillations in a single rectangular bay based on the Boussinesq equations. In their analysis the wave field in the ocean is approximated by a linear theory. They demonstrated, with the support of their own experimental data, that through the nonlinearity, large higher harmonics are generated when the first harmonic of the incident waves is resonated inside the bay. More recently, *Woo and Liu* [2004a, 2004b] developed a transient finite element model based on the modified Boussinesq equations [*Nwogu*, 1993] and revisited R&M's problem. They confirmed that the approximations adopted in R&M, such as the linearization of the wave field outside the bay, are acceptable. The finite element solutions seem to agree slightly better with the experimental data for the second and third harmonics.

[1] Also at Department of Physics, University of the Balearic Islands, Palma, Balears, Spain.

0148-0227/04/2003JC002039

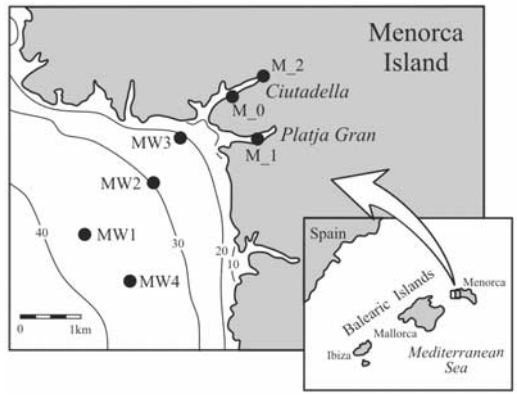

Figure 1. Geometry and location of Ciutadella and Platja Gran, Menorca Island, in the western Mediterranean and location of the instruments deployed during LAST-97. Depths are labeled in meters.

[4] In many places around the world, one can easily find locations where two bays are located very close to each other. For example, Ciutadella and Platja Gran are two elongated bays on the west coast of Menorca, on the Balearic Islands in the western Mediterranean (Figure 1). Large oscillations (up to 3 m in wave height) are periodically observed in both bays. These large oscillations, locally known as 'rissaga', have been linked to the passage of atmospheric pressure disturbances, which generate long ocean waves on the continental shelf surrounding the islands that, in turn, force the resonance response in these bays [*Tintoré et al.*, 1988; *Monserrat et al.*, 1991; *Gomis et al.*, 1993; *Rabinovich and Monserrat*, 1998]. Using linear shallow water equations, *Liu et al.* [2003, 2004] examined the coupled oscillations in these bays. They selected a background period of relatively weak bay oscillations, when the significant wave heights inside the bays are in the order of magnitude of few centimeters and the measured wave heights on the shelf are one order of magnitude smaller. Considering the wave period of the lowest-resonance mode (about 10 min), the corresponding wavelength is about 10 km in the water depth of 30 m (on the shelf) and 4 km in the water depth of 5.5 m (inside the bays), respectively. Therefore the wave system studied by *Liu et al.* [2003, 2004], even under the resonance condition, was indeed linear. Their results, which agree with many features observed in the field data, show that the coupling is primarily due to the radiated waves propagating from one bay to the other. The coupling effects become stronger when two bays are closer. However, during a rissaga event, oscillations inside the bays may reach wave heights of more than 3 meters in the averaged water depth of 5.5 meter and, therefore nonlinear effects should play a significant role.

[5] The main goal of this paper is to examine theoretically the nonlinear coupling of two adjacent bays and to use the model as a tool to interpret the nature of the nonlinear coupling of Ciutadella and Platja Gran during a rissaga event. To simplify the problem, we shall assume that both bays are elongated rectangles, of constant depth and perpendicular to the coastline. We shall extend R&M's approach to the new system and reduce the Boussinesq equations to a set of coupled two-point boundary value problems for each harmonic motion in each bay. A numerical algorithm is developed to solve the system of nonlinear second-order boundary value problems. Present numerical results are first compared with R&M's numerical results and experimental data for a single bay. The discrepancies among the results are discussed. The response curves for the first three harmonics, evaluated at the end of the bay, are also obtained for a range of incident frequencies. The effects of nonlinearity on the resonance of higher harmonics are illustrated. Solutions for the two bays system, in which one bay length is twice the other one, are later obtained and discussed. The response curves for each harmonic in each bay are also calculated. Special attention is focused on the effects of nonlinearity and resonance coupling. Amplification curves are computed and compared with data in the region of Ciutadella under almost linear and fully nonlinear conditions.

2. Field Evidence

[6] The LAST-97 field experiment was carried out in the region of Ciutadella from June to September 1997. A set of bottom pressure recorders and microbarographs was deployed. Bottom pressure recorders were installed inside the Ciutadella Inlet, one near the middle (M_0) and the other one close to the end of the inlet (M_2), near the middle of the neighboring inlet of Platja Gran (M_1) and on the outer shelf of Menorca Island (bottom pressure gauges MW1, MW2, MW3 and MW4) (see Figure 1). All bottom pressure gauges recorded continuously for 30 seconds s intervals and stored the data with a sampling interval Δt = 1 min.

[7] During the field observation period, the instruments located in Ciutadella Inlet and over the shelf captured several rissaga events. However, M_1 instrument was temporally out of order during the first part of the field observation and only one of these events was simultaneously recorded in Platja Gran. In addition, some periods of extremely low activity, with significant wave heights inside the inlets in the order of magnitude of only few centimeters, were also identified.

[8] The most energetic events were selected and analyzed by *Monserrat et al.* [1998] and compared with a period of low activities (background) by using spectral techniques. *Liu et al.* [2003, 2004] further investigated the background case showing evidences of resonant linear coupling between the inlets.

[9] Here, the most energetic event, simultaneously recorded in both inlets, is selected and compared with a period of background oscillations. In order to increase the confidence of analyses, an additional event, representing an intermediate energetic state is also considered. The three events have been selected with the same duration interval of 5760 min (4 days) and are (1) background: 27–31 July, maximum wave height 5 cm; (2) rissaga: 21–25 July, maximum wave height 125 cm; and (3) intermediate: 16–20 August, maximum wave height 25 cm.

[10] The analysis of these episodes is carried out by computing the spectral contents for each instrument, inside Ciutadella and Platja Gran Inlets and on the shelf. A Kaiser-Bessel window of 512 points with half-window overlapping was used for all the computations [*Emery*

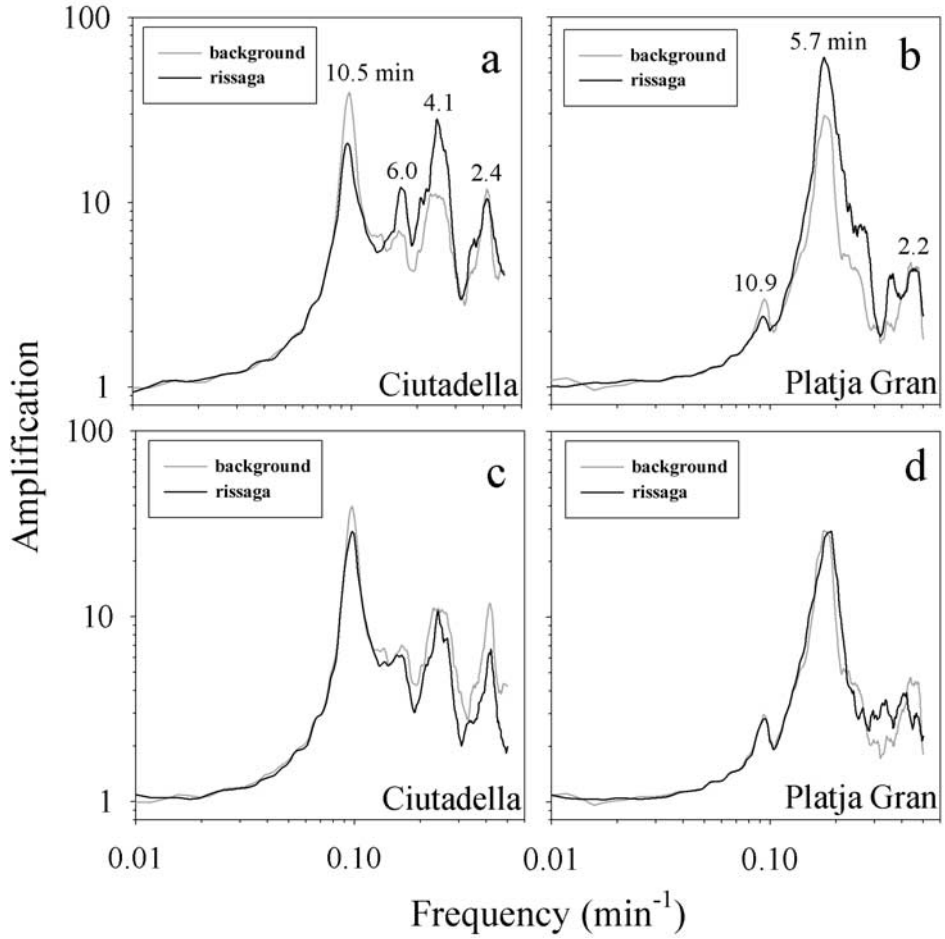

Figure 2. Relative amplification at (a) Ciutadella and (b) Platja Gran computed for the background period (shaded lines) and rissaga (black lines). The same background episode is compared with the intermediate case at (c) Ciutadella and (d) Platja Gran. Major peaks are labeled with the corresponding period in minutes.

and Thomson, 1997], resulting in 42 degrees of freedom (dof).

[11] In order to filter out the shelf resonance characteristics affecting the instruments inside the inlets, the spectra at the inlet sites are divided by the spectrum at one of the instruments on the shelf. The square root of this ratio may be considered as a good estimation of the inlet admittance function, i.e., as the relative amplification of the waves, arriving from the shelf, inside the inlet. Instrument MW4 is selected as the representative of shelf oscillations. Although it is located relatively far away from the inlet entrances it is expected that this instrument will be less affected by radiated waves from the inlets.

[12] The amplification functions at M_1 and M_2 during the rissaga and the intermediate episodes are compared with those during the background and are shown in Figure 2. The background responses have been analyzed in detail by *Liu et al.* [2003, 2004]. The amplifications are clearly different in the two inlets. The fundamental and first resonant periods for Ciutadella are 10.5 and 4.1 min, while the fundamental and first resonant periods for Platja Gran are 5.7 and 2.2 min. Some other minor disturbances of the amplification curves, located at the resonance frequencies of the neighboring inlet are also clear. *Liu et al.* [2003, 2004] called the presence of these disturbances in the background case as coupled modes. The gross behavior of the amplification for all three cases is similar; in particular, resonant peaks are located at the same frequencies. However, the magnitudes of the amplification peaks are different. The amplification at the fundamental mode in Ciutadella is smaller during rissaga, on the other hand, the amplification of the fundamental mode in Platja Gran is considerably greater. Higher-order resonant modes in both inlets increase their magnitudes during rissaga. Similar features are also observed for the intermediate case, although the changes of the fundamental mode amplifications are less evident. It is suggested this is due to the fact that the fundamental resonant mode in Platja Gran (T_0 = 5.7 min), is close to the second harmonic of the Ciutadella fundamental resonant mode (T_0 = 10.5 min). The detailed discussion and explanation of this feature is the main thrust of the paper.

3. Analytical Formulation

[13] The inlet geometry for Ciutadella and Platja Gran can be approximated by two rectangular and parallel bays with constant water depth *h*. We consider two adjacent bays

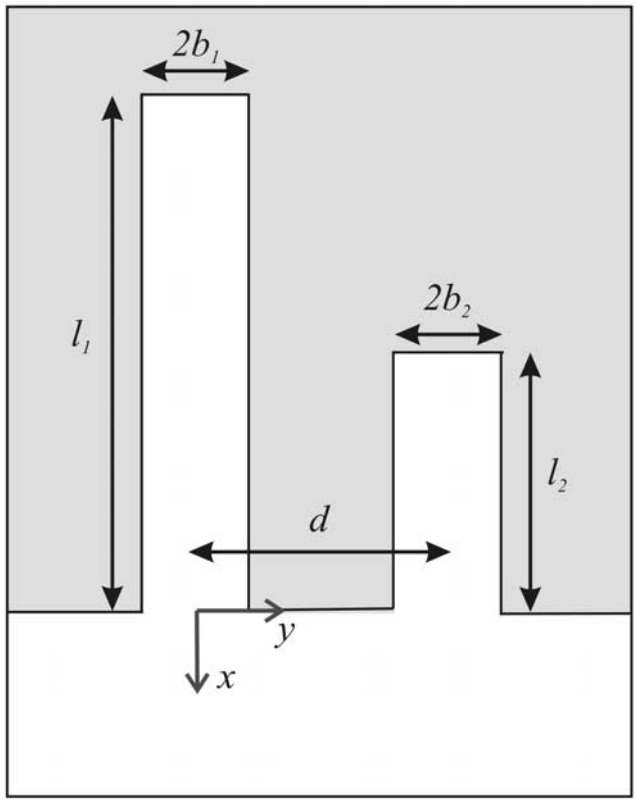

Figure 3. Definition sketch of idealized geometry for two rectangular bays.

with lengths, l_1 and l_2, and width $2b_1$ and $2b_2$, respectively. The coastline is a straight line and coincides with the y axis. Both bays are perpendicular to the coast and are aligned with the x axis. The water depth is constant everywhere (see Figure 3). An incident wave train propagates normally to the coast from x $\rightarrow \infty$. Adopting the following dimensionless variables:

$$t' = \omega t, (x', y') = (x, y)\frac{\omega}{\sqrt{gh}}, z' = \frac{z}{h}, \zeta' = \frac{\zeta}{h}, \mathbf{u}' = \frac{\mathbf{u}}{\sqrt{gh}}, \quad (1)$$

in which ω is the characteristic wave frequency, and g the gravity acceleration. The well-known Boussinesq equations for free surface displacement, ζ, and horizontal velocity vector, $\mathbf{u}$, can be written in the dimensionless form as follows:

$$\zeta_t + \nabla \cdot \mathbf{u} + \nabla \cdot (\zeta \mathbf{u}) = 0 \quad (2)$$

$$\mathbf{u}_t + \nabla\zeta + \frac{1}{2}\nabla\mathbf{u}^2 + \frac{1}{3}\mu^2\nabla\zeta_{tt} = 0, \quad (3)$$

in which $\mu^2 = \omega^2 h/g \ll 1$ represents the frequency dispersion. In the above equations the primes have been dropped for all dimensionless variables. These equations have been derived assuming that earth rotation is negligible and ignoring frictional effects. We should also point out that the dimensionless free surface elevation, ζ, and velocity, $\mathbf{u}$, are in the order of O(ε), representing the nonlinearity parameter. The Boussinesq approximation requires that both ε and μ^2 are small and are in the same order of magnitude. The errors of the above equations are of the order of O(ε^2, $\varepsilon\mu^2$, ε^4).

[14] Because of the nonlinearity, the bay responses are expected to contain higher harmonics. Therefore we seek for the following solution forms:

$$\zeta = \frac{1}{2}\sum_n \zeta_n(x,y)e^{-\mathrm{int}}, \quad \mathbf{u} = \frac{1}{2}\sum_n \mathbf{u}_n(x,y)e^{-\mathrm{int}}, \quad (4)$$

where n = 1, 2, 3, . . ., ζ_{-n} and $\mathbf{u}_{-\mathrm{n}}$ are the complex conjugates of ζ_n and $\mathbf{u}_{\mathrm{n}}$, respectively. Substituting equation (4) into equations (2) and (3) results in a set of governing equations for each harmonic

$$-in\zeta_n + \nabla \cdot \mathbf{u}_n + \frac{1}{2}\sum_s \nabla \cdot (\zeta_s \mathbf{u}_{n-s}) = 0 \quad (5)$$

$$-in\mathbf{u}_n + \left(1 - \frac{1}{3}\mu^2 n^2\right)\nabla\zeta_n + \frac{1}{4}\sum_s \nabla(\mathbf{u}_s \cdot \mathbf{u}_{n-s}) = 0. \quad (6)$$

These two equations can be combined by taking the divergence of equation (6) and multiplying equation (5) by a factor $i{\cdot}n$. Adding the resulting equations one easily gets

$$(\nabla^2 + k_n^2)\zeta_n = \sum_s \left[-\frac{i}{2}n\nabla \cdot (\zeta_n \mathbf{u}_{n-s}) - \frac{1}{4}\nabla^2(\mathbf{u}_s \cdot \mathbf{u}_{n-s})\right], \quad (7)$$

where

$$k_n^2 = \frac{n^2}{1 - \frac{1}{3}\mu^2 n^2}. \quad (8)$$

This equation represents a system of coupled nonlinear wave equations. If the nonlinearity is insignificant, the system is decoupled and the wave number for each harmonic is slightly influenced by the frequency dispersion, i.e., from equation (8) $k_n \approx n(1 + \mu^2 n^2/6)$.

[15] In the remainder of this section, we shall present first the approximate solutions inside the bays and in the ocean. We shall follow R&M's arguments [see also *Mei*, 1989, p. 593] that the nonlinearity is only important inside the bays. The wave field in the ocean and the matching conditions near the bay entrance can be approximated by linear theory.

3.1. Solution in the Ocean

[16] Within the framework of the linear wave theory, the free surface profile in the ocean can be viewed as the sum of the incident wave, the reflected wave from the coast, and the radiated wave from the bay entrances. Thus

$$\zeta_n^0 = A_n \cos k_n x + \zeta_n^R, \quad (9)$$

where A_n is twice of the incident wave amplitude for the nth harmonic and ζ_n^R denotes the radiated wave from both bays. Once again, if the width of each bay is small in comparison with the bay length and the incident wavelength and if the

distance between these two bays is larger than the wavelength, we can obtain the radiated wave solution by treating the bay entrances as two oscillatory point sources. Thus

$$\zeta_n^R = \frac{nQ_n^{(1)}}{2} H_0^{(1)}(k_n r_1) + \frac{nQ_n^{(2)}}{2} H_0^{(1)}(k_n r_2) \tag{10}$$

with

$$r_1 = \sqrt{x^2 + y^2} \quad and \quad r_2 = \sqrt{x^2 + (y-d)^2} \tag{11}$$

and $Q_n^{(1)}$ and $Q_n^{(2)}$ are the volume fluxes for the nth harmonic through the bay entrances at $r_1 = 0$ and $r_2 = 0$, respectively, and $H_0^{(1)}$ is the Hankel function of the first kind and of order zero. The distance between the bay entrances has been denoted by d. Far away from the bay entrances, r_1, $r_2 \to \infty$, the Hankel functions behave as periodic functions in $k_n r_1$ and $k_n r_2$, respectively, representing outgoing waves.

[17] To find $Q_n^{(1)}$ and $Q_n^{(2)}$ the solutions on the ocean side need to be matched with the solutions inside the bays. The matching will be done asymptotically. Thus we need to find the inner expansions of the radiated waves in the vicinity of each bay entrance. Near the entrance of the first bay ($r_1 = 0$), the asymptotic expansion of equation (10) can be obtained by letting $k_n r_1$ go to zero. Hence

$$\zeta_n^R \approx \frac{nQ_n^{(1)}}{2}\left(1 + \frac{2i}{\pi}\ln\frac{\gamma k_n r_1}{2}\right) + \frac{nQ_n^{(2)}}{2} H_0^{(1)}(k_n r_2), k_n r_1 \approx 0. \tag{12}$$

Similarly, near the entrance of the second bay ($r_2 = 0$), the inner expansion becomes

$$\zeta_n^R \approx \frac{nQ_n^{(2)}}{2}\left(1 + \frac{2i}{\pi}\ln\frac{\gamma k_n r_2}{2}\right) + \frac{nQ_n^{(1)}}{2} H_0^{(1)}(k_n r_1), k_n r_2 \approx 0, \tag{13}$$

in which $\ln\gamma = 0.5772157$. The logarithmic singularities at $r_1 = 0$ and $r_2 = 0$ confirm that the wave field behaves like an oscillatory point source at the bay entrance. The inner expansions of the wave field in the ocean toward the bay entrances become

$$\zeta_n^0 \approx A_n + \zeta_n^R, \tag{14}$$

in which ζ_n^R is given by either equation (12) or equation (13). While the incident wave heights A_n are known quantities, $Q_n^{(1)}$ and $Q_n^{(2)}$ need to be determined through matching.

3.2. Solution in the Bays

[18] Because of the narrowness of the bay width as compared to the characteristic wavelength, the nth harmonic free surface displacement can be considered as independent of y. Therefore equation (7) becomes

$$\frac{d^2\zeta_n}{dx^2} + k_n^2\zeta_n = \sum_s \left[\frac{-i}{2} n \frac{d(\zeta_n u_{n-s})}{dx} - \frac{1}{4}\frac{d^2(u_s u_{n-s})}{dx^2}\right], \tag{15}$$

where, now, u_s and u_{n-s} are one dimensional velocities. On the other hand, from equations (5) and (6) is deduced that

$$\begin{aligned} \frac{du_n}{dx} &= in\zeta_n(1 + o(\varepsilon)) \\ u_n &= -\frac{i}{n}\frac{d\zeta_n}{dx}(1 + o(\varepsilon)) \end{aligned}. \tag{16}$$

Using these expressions, the right hand side terms of equation (15) can be simplified in the following manner:

$$\begin{aligned} \sum_s \frac{d(\zeta_n u_{n-s})}{dx} &= \sum_s \left[\zeta_n \frac{du_{n-s}}{dx} + \frac{d\zeta_n}{dx} u_{n-s}\right] \\ &= \sum_s \left[\zeta_n i(n-s)\zeta_{n-s} + \frac{d\zeta_n}{dx}\frac{-i}{n-s}\frac{d\zeta_{n-s}}{dx}\right] \end{aligned} \tag{17}$$

$$\begin{aligned} \sum_s \frac{d^2(u_s u_{n-s})}{dx^2} &= \sum_s \left[u_s \frac{d^2 u_{n-s}}{dx^2} + \frac{d^2 u_s}{dx^2} u_{n-s}\right] \\ &= \sum_s \left[\frac{s}{n-s}\frac{d\zeta_s}{dx}\frac{d\zeta_{n-s}}{dx} - (n-s)\zeta_{n-s}\zeta_s\right]. \end{aligned} \tag{18}$$

The substitution of equations (17) and (18) into equation (15) provides the final expression for the sea level variation:

$$\begin{aligned} \frac{d^2\zeta_n^{(j)}}{dx^2} + k_n^2\zeta_n^{(j)} &= \frac{1}{2}\sum_s \left(n^2 - s^2\right)\zeta_s^{(j)}\zeta_{n-s}^{(j)} \\ &\quad - \frac{1}{2}\sum_{s\neq n} \frac{n+s}{n-s}\frac{d\zeta_s^{(j)}}{dx}\frac{d\zeta_{n-s}^{(j)}}{dx} \quad j = 1, 2, \end{aligned} \tag{19}$$

which is a system of coupled second-order ordinary differential equations in terms of different free surface harmonics inside each bay. To find solutions for these equations, boundary conditions are required. At the end of each bay, the no-flux boundary condition is imposed, i.e.,

$$\frac{d\zeta_n^{(j)}}{dx} = 0, \quad x = -l_j, \tag{20}$$

where $j = 1, 2$ denoting the jth bay. Near the bay entrance, the solutions obtained from equation (19) must be matched with the solutions in the vicinity of the bay entrances, where the flow field is no longer one dimensional. To perform the asymptotic matching, the asymptotic expression of the wave field as $kx \to 0$ can be written in terms of a Taylor's series expansion,

$$\zeta_n^{(j)} \approx \zeta_n^{(j)}(0) + x\frac{d\zeta_n^{(j)}}{dx} + \dots . \tag{21}$$

To connect the wave field in the ocean and those in the bays, we need to find the approximate solutions in the vicinity of bay entrances. Because the width of the bay is narrow, flow motions near the bay entrances (the near field) are governed by the Laplace equation. Therefore, for the right-angled bay entrance the solutions for the flow field can be obtained via the conformal mapping method. The details of the solution finding procedure are given by *Mei* [1989, p. 199] and will not be repeated here. Only the

outer expansions of the near field solutions for the nth harmonic are given here.

$$\zeta_n^{(j)} \approx M_j \frac{\pi x}{2b_j} - M_j \ln\left(\frac{e}{2}\right) + C_j, \quad x < 0 \tag{22}$$

$$\zeta_n^{(j)} \approx M_j \ln\left(\frac{\pi r_j}{2b_j}\right) + C_j, \quad x > 0. \tag{23}$$

Physically, while the near field solution on the bay side represents oscillatory uniform flow in the x direction, on the ocean side the solution denotes an oscillatory point source. Matching of the inner and outer solutions on the bay sides and the ocean side, i.e., matching equation (21) with equation (22) and equation (14) with equation (23), yield a set of eight linear algebraic equations for ten unknown quantities, M_j, C_j, $Q_n^{(j)}$, $\zeta_n^{(j)}(0)$ and $d\zeta_n^{(j)}(0)/dx$. After some lengthy, but straightforward manipulations, we find the following important relationships at the bay entrances:

$$\frac{in}{k_n^2} Z_n^{(1)} \frac{d\zeta_n^{(1)}(0)}{dx} + \zeta_n^{(1)}(0) = -ib_2 H_0^{(1)}(k_n d) \frac{d\zeta_n^{(2)}(0)}{dx} + A_n \tag{24}$$

$$\frac{in}{k_n^2} Z_n^{(2)} \frac{d\zeta_n^{(2)}(0)}{dx} + \zeta_n^{(2)}(0) = -ib_1 H_0^{(1)}(k_n d) \frac{d\zeta_n^{(1)}(0)}{dx} + A_n, \tag{25}$$

where

$$Z_n^{(j)} = \frac{k_n^2 b_j}{n} \left[1 + \frac{2i}{\pi} \ln\left(\frac{2\gamma k_n b_j}{\pi e}\right)\right] \qquad j = 1, 2 \tag{26}$$

is the entrance impedance for each bay in the absence of the other bay. In summary, equation (19) represents a set of second-order, nonlinear ordinary partial differential equations for $\zeta_n^{(j)}$ inside the bays. Equations (24), (25), and (20) constitute the necessary boundary conditions for equation (19) as a set of two-point boundary value problems.

[19] The zeroth harmonic solutions correspond to mean sea level changes and mean current, which can be obtained by integrating the one-dimensional version of equations (5) and (6) for each bay

$$u_0^{(j)} = -\frac{1}{2} \sum_s \zeta_s^{(j)} u_{-s}^{(j)} \tag{27}$$

$$\zeta_0^{(j)} = -\frac{1}{4} \sum_s \left|u_s^{(j)}\right|^2 + c_j, \tag{28}$$

where c_j (j = 1, 2) are constants to be determined. We remark here that the current velocity has satisfied the no-flux conditions at the end of each bay. Assuming that the mean sea level outside the bays has been properly adjusted so that $A_0 = 0$, we can readily show that the impedance conditions (24) and (25) are satisfied for n = 0, with $c_j = 0$. Therefore the mean free surface displacement and the mean velocity are of the order of $O(\varepsilon^2)$ and will be ignored in the nonlinear equations for other harmonics.

[20] Although the Fourier series in equation (19) are infinite, we consider here that the response is only appreciable in the first three harmonics. For later use, the governing equations for each of these harmonics in each bay can be written in the following explicit forms.

$n = 1$:

$$\frac{d^2\zeta_1^{(j)}}{dx^2} + k_1^2 \zeta_1^{(j)} = -\frac{3}{2}\left(\zeta_2^{(j)}\zeta_{-1}^{(j)} + \zeta_{-2}^{(j)}\zeta_3^{(j)}\right) - 4\zeta_3^{(j)}\zeta_{-2}^{(j)} + \frac{3}{2}\frac{d\zeta_2^{(j)}}{dx}\frac{d\zeta_{-1}^{(j)}}{dx} + \frac{7}{6}\frac{d\zeta_{-2}^{(j)}}{dx}\frac{d\zeta_3^{(j)}}{dx}, \tag{29}$$

$n = 2$:

$$\frac{d^2\zeta_2^{(j)}}{dx^2} + k_2^2 \zeta_2^{(j)} = \frac{3}{2}\zeta_1^{(j)}\zeta_1^{(j)} - \zeta_3^{(j)}\zeta_{-1}^{(j)} - \frac{3}{2}\frac{d\zeta_1^{(j)}}{dx}\frac{d\zeta_1^{(j)}}{dx} + \frac{7}{3}\frac{d\zeta_3^{(j)}}{dx}\frac{d\zeta_{-1}^{(j)}}{dx}, \tag{30}$$

$n = 3$:

$$\frac{d^2\zeta_3^{(j)}}{dx^2} + k_3^2 \zeta_3^{(j)} = \frac{13}{2}\zeta_1^{(j)}\zeta_2^{(j)} - \frac{7}{2}\frac{d\zeta_1^{(j)}}{dx}\frac{d\zeta_2^{(j)}}{dx}. \tag{31}$$

They form, together with their complex conjugates, a second-order nonlinear coupled system of 12 equations.

4. Numerical Resolution of the Two-Point Boundary Value Problem

[21] The two-point boundary value problem derived in the previous section is solved numerically by using the shooting method [*Press et al.*, 1989]. To do so, the second-order differential equation system is first converted into a system of first-order differential equations. This can be accomplished by introducing new variables $\eta_n^{(j)} = d\zeta_n^{(j)}/dx$ and $d\eta_n^{(j)}/dx = d^2\zeta_n^{(j)}/dx^2$. By substitutions, equations (29), (30), and (31) are converted into a system of first-order differential equations in terms of $\eta_n^{(j)}$ and $\zeta_n^{(j)}$ for $n = 1, 2, 3$ and $j = 1, 2$. Therefore, if only the first three harmonics are considered, there are 12 resulting equations. Similarly, the boundary conditions can also be expressed in terms of the new variables. Since the numerical algorithm for the shooting method adopted in this paper only deals with real variables, the governing equations and boundary equations, which are all written in terms of complex variables, are further decomposed into real and imaginary parts. The final governing equations consist of 24 coupled first-order differential equations for $\mathrm{Re}(\eta_n^{(j)})$, $\mathrm{Im}(\eta_n^{(j)})$, $\mathrm{Re}(\zeta_n^{(j)})$ and $\mathrm{Im}(\zeta_n^{(j)})$ with 12 boundary conditions at x = 0 and other 12 boundary conditions at $x = -l_j$.

[22] The shooting method employed is a standard method and will be only briefly described here. In this method, we first choose a set of values for all variables at the boundary, $x = -l_j$, which, however, must be consistent with the no-flux boundary conditions (i.e., $\zeta_n^{(j)} = 0$). Therefore there are only 12 free initial guesses at the first boundary. These initial guesses are used to integrate the system of ordinary differential equations as an initial value problem until arriving at the other boundary, x = 0. The integration is done by means

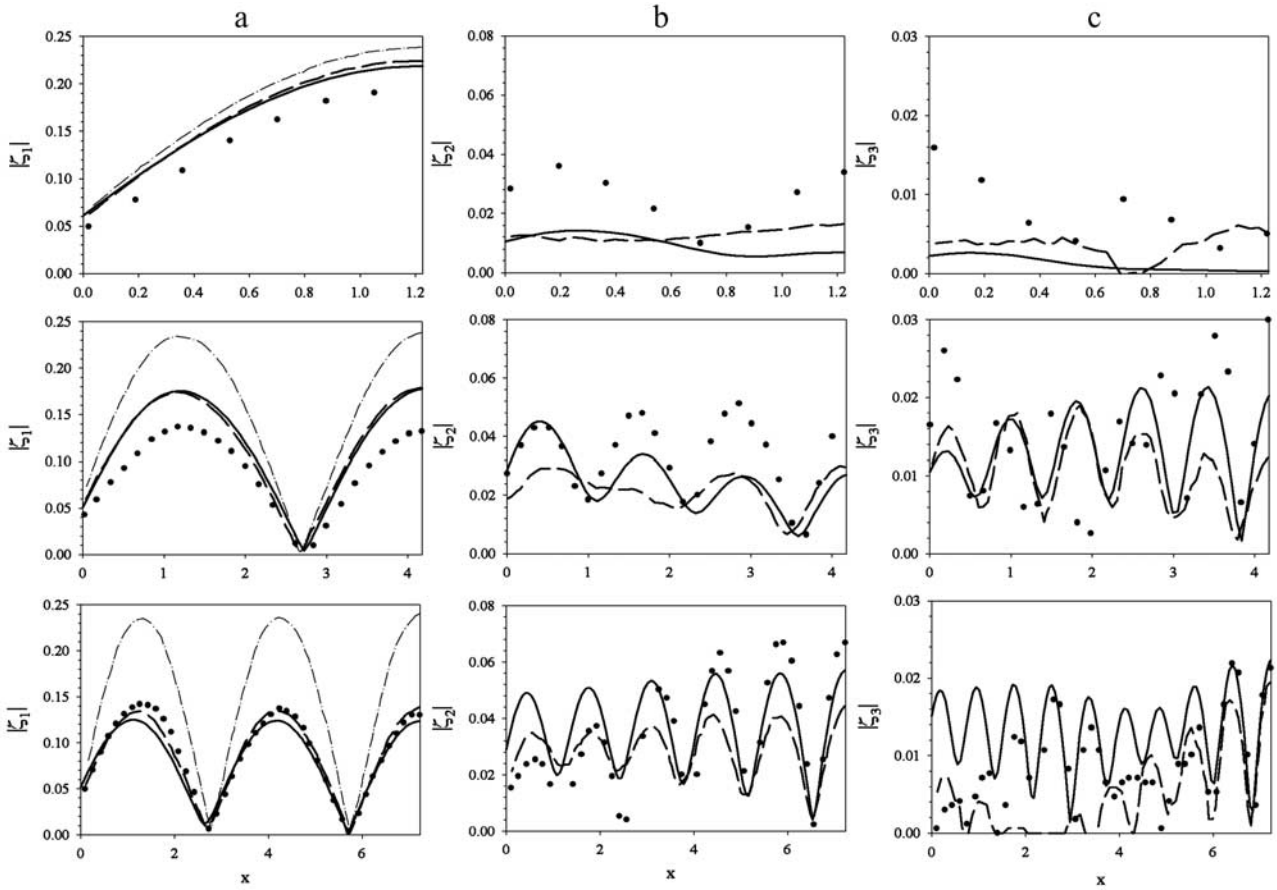

Figure 4. Dimensionless amplitudes in a single bay for the (a) first, (b) second, and (c) third harmonic for three resonant bay lengths, coinciding with those used in R&M: 1.227, 4.23, and 7.233. Solid lines represent the present results; dashed lines are the results obtained by R&M; dots are experimental data. The results for the first harmonic are also compared with the linear solutions (dot-dashed lines).

of a fifth-order Runge-Kutta method, which adjusts the integration step size and monitors local truncation error. At x = 0 we define a discrepancy vector **F**, whose dimension is 12 and whose components measure the residues of the boundary conditions at x = 0. A globally convergent Newton's method is used to find the initial values for which the discrepancy vector F becomes negligible.

5. Results and Discussions

[23] Results are obtained for several problems, including almost linear and fully nonlinear oscillations in a single bay and nonlinear coupling between two adjacent bays. Some of these cases, such as the single bay problem, have been studied by other researchers and are reexamined here for the purpose of confirming the accuracy of the present numerical algorithm and establishing the background information for further discussions on nonlinear coupling phenomena.

5.1. Nonlinear Oscillations in a Single Bay

[24] R&M's numerical solutions for the nonlinear oscillations in a single rectangular bay are based on a similar formulation shown in this paper. However, their numerical integration technique, the method of complementary functions, is different from the shooting method used here. In R&M, laboratory experiments were also performed for three different bay lengths, which correspond to the first three resonant modes of the first harmonic with the fixed incident frequency $\omega = 4.067\ s^{-1}$. For each bay length three different incident wave amplitudes were tested. The numerical values for the dimensionless parameters are: l = 1.227, 4.230, 7.233; b = 0.169; A_1 = 0.015, 0.027, 0.040. We remark here that for these experiments while the dispersion parameter is fixed at $\mu^2 = 0.257$ for all cases, the nonlinearity ε varies from 0.015 to 0.04 in the open ocean. Since the waves inside the bay are resonated, the nonlinearity becomes the same order of magnitude of the frequency dispersion and both are quite significant.

[25] To ensure that our numerical algorithm is correctly implemented, R&M's cases are recalculated and the numerical results are compared with their experimental data and numerical solutions as well. In order to compare both numerical solutions we have used an approximate expression for the wave number, following R&M: $k_n^2 = n^2(1 + {}^1/_3\mu^2 n^2)$. To obtain numerical solutions for a single bay from the present formulation for a two-bay system, we just need to set the length and width of the second inlet equal to zero. Here only the case with the largest amplitude ($A_1 = 0.04$ or $\varepsilon = 0.04$) is shown (see Figure 4). For the first harmonic (Figure 4a), the numerical solutions obtained by R&M and the present numerical solutions are very similar. For the two shorter bays they are slightly higher than the

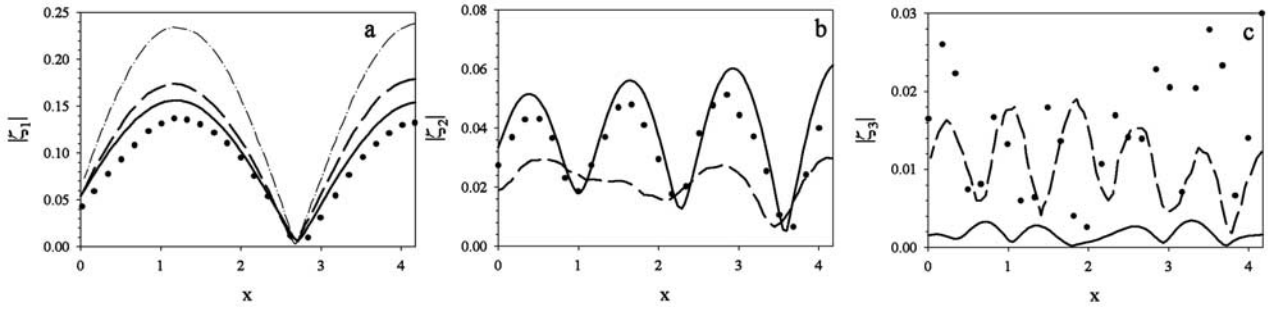

Figure 5. Dimensionless amplitudes in a single bay of length 4.230 for the (a) first, (b) second, and (c) third harmonics. Solid lines represent the present results computed with the complete expression for the wave number; dashed lines are the results obtained by R&M; dots are experimental data. The results for the first harmonic are also compared with the linear solutions (dot-dashed lines).

experimental data. As pointed out in R&M these discrepancies could be due to the lack of inclusion of physical dissipative mechanisms in the theoretical formulation. However, for the longest bay (Figure 4a (bottom)), solutions are very close to the experimental data. The higher harmonics show larger discrepancies between R&M's computations and ours. These differences are due to the different numerical methods used for solving the system of equations. In the case of the second harmonic of shortest bay (Figure 4b (top)), differences between experimental data and numerical solutions are relatively significant. The solutions for the third harmonic are also shown in the same figure (Figure 4c). However, the magnitude of their amplitudes is very small and the resolution of the experimental data is too poor to make a serious comparison.

[26] The approximated expression for the wave number used in these computations is valid when the frequency dispersion effects are negligible. However, the dispersion parameter used in the experimental setup is too large to be considered insignificant. New computations using the complete expression for the wave number, given by equation (8), are plotted in Figure 5 for the second bay length. The first harmonic is now closer to the experimental data, although it is still larger. For the second harmonic, experimental data are better reproduced by these numerical solutions (Figure 5b); namely, amplitude envelopes of the second harmonic decay slightly from the end of the bay toward the mouth of the bay. On the other hand, R&M's solutions did not capture this feature.

[27] Because of the nonlinearity second harmonic and third harmonics are generated. It is therefore not surprising that the amplitude of the first harmonic, based on the nonlinear theory, is smaller than the amplitude calculated from the linear theory (Figure 4a). It is also true that the efficiency of radiation damping, which is proportional to $k_n b \ln(k_n b)$, equation (26), is higher for higher harmonics. Therefore the total response based on the nonlinear theory maybe lower than that calculated from the linear theory.

[28] To further explore the nonlinear effects, response curves for each harmonic are calculated in the frequency range between $k_1 l = 0.1$ and $k_1 l = 10$, corresponding to $4.7 \times 10^{-5} < \mu^2 < 0.47$ with l being the longest bay length in R&M's experiments. The response curve is the amplitude of each harmonic at the end of each bay, normalized y the incident wave height, i.e., $|\zeta_1|/A_1$, $|\zeta_2|/A_1$, $|\zeta_3|/A_1$. Here two cases are considered: one for small amplitude incident waves $A_1 = 0.01$ and $A_2 = A_3 = 0$, and the second for finite amplitude waves $A_1 = 0.1$ and $A_2 = A_3 = 0$. The response curves are shown in Figure 6.

[29] It is well known that for a narrow rectangular bay the resonant modes can be roughly estimated as $k_1 l = (n + 1/2)\pi$, $n = 0, 1, 2, 3$. The fundamental ($n = 0$), first ($n = 1$)

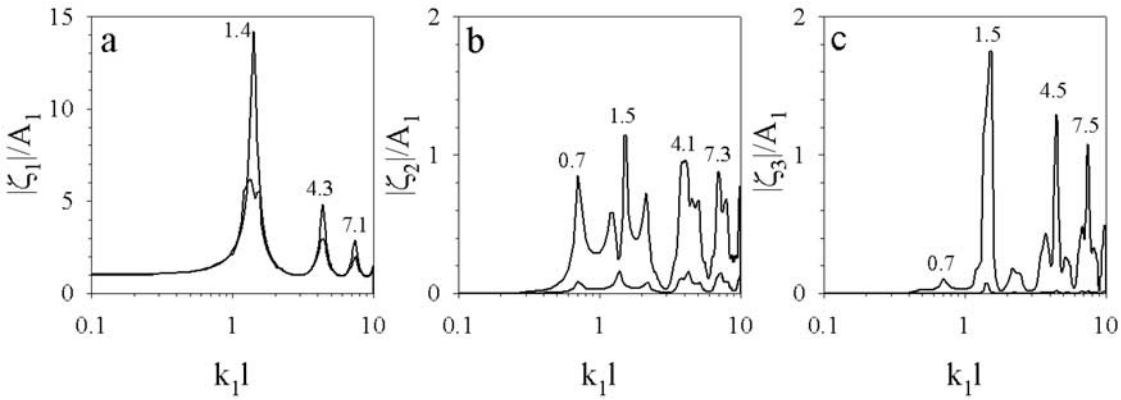

Figure 6. Amplification factors for the (a) first, (b) second, and (c) third harmonics in a single bay. Results with $\varepsilon = 0.01$ (shaded line) and $\varepsilon = 0.1$ (black line) are shown. Numerical values denote the peak frequencies in terms of $k_1 l$.

and second ($n = 2$) resonant modes are approximately equal to 1.57, 4.71, 7.85. Note that the first mode frequency is exactly three times the fundamental mode in this rough estimation. However, slight shifts of these resonant frequencies due to radiation damping and nonlinearity are also anticipated. These resonant modes are well represented by the linear solutions of the first harmonic shown in Figure 6a, i.e., $k_1 l = 1.4$, 4.3 and 7.1. When the nonlinearity is important, higher harmonics are generated. And when the incident wave frequency is one half of the fundamental resonant frequency, the second harmonic of the incident wave is expected to be resonated inside the bay. This explains the appearance of the resonance peak of the second harmonic amplification factor at $k_1 l \sim 0.7$ in Figure 6b. For the same reason another resonance peak shows up in the response curve of the second harmonic at $k_1 l \sim 2.1$, which is roughly one half of the first resonant frequency, $k_1 l \sim 4.3$. As discussed before that one third of the first resonant frequency is approximately the same as the fundamental resonance frequency. Therefore, if the incident wave frequency is around $k_1 l \sim 1.5$ the corresponding third harmonic is resonated (see Figure 6c). We should also point out that the fundamental resonance frequency has shifted to $k_1 l = 1.2$. Similar features also occur in the neighborhood of higher resonant modes. For instance, when the incident wave frequency is around $k_1 l \sim 3.6$, the corresponding second harmonic has the frequency of $k_1 l \sim 7.2$, which is very close to the second resonance mode of the bay. Therefore the second harmonic is resonated and contributes to almost one third of the total response at $k_1 l \sim 3.6$ (see Figure 6b).

5.2. Nonlinear Coupling for Two Adjacent Bays

[30] Within the framework of linear shallow water theory, *Liu et al.* [2003, 2004] presented analytical solutions for coupled oscillations in two adjacent rectangular bays. A set of geometrical and wave parameters were chosen in their calculations for the amplification factors of each bay. These parameters are representative of Ciutadella and Platja Gran as shown in Figure 1 under the background wave conditions (i.e., very small incident wave heights) and are given as $l_1 = 1000$ m, $l_2 = 0.5 l_1$, $b_1 = b_2 = 0.05 l_1$, $h = 5.5$ m, $d = 0.1 l_1$. Response curves were again calculated in the frequency range, $0.1 < k_1 l_1 < 10$, corresponding to $3.0 \times 10^{-7} < \mu^2 < 3.0 \times 10^{-3}$. It is obvious that within this frequency range, the frequency dispersion effects are insignificant. Since the incident wave height is also very small, $A_1 = 0.01$ and $A_2 = A_3 = 0$, the Boussinesq equations reduce to the linear shallow water equations.

[31] In Figure 7 the individual response curves, $|\zeta_1|/A_1$, $|\zeta_2|/A_1$, $|\zeta_3|/A_1$, for both bays are plotted for linear ($A_1 = 0.01$, shaded lines) and nonlinear waves ($A_1 = 0.1$, black lines). For the small incident wave the responses of the second and third harmonics are negligible. The total response curve is almost entirely due to the first harmonic. The linear solutions indicate again that in the first (longer) bay the first three resonant modes are $k_1 l_1 = 1.4$, 4.3, and 7.1 (Figure 7a (top)), which are the same as those for a single bay (see Figure 6). The response curve is distorted between the fundamental and the first resonant mode of the first bay at a frequency around $k_1 l_1 = 2.6$ which corresponds to the fundamental mode of the second (shorter) bay. In the second bay (Figure 7b (top)), the fundamental resonant mode is indeed located at $k_1 l_1 = 2.6$. We remark here that because the length of the shorter bay is exactly one half of the length of the longer bay. Therefore, on the basis of the single bay results the fundamental resonance frequency for the shorter bay should be $k_1 l_2 \sim 1.4$, which leads to $k_1 l_1 \sim 2.8$. The slight difference between the rough estimation (2.8) and the actual calculated value (2.6) is caused by the interference of two bays. In the response curve for the shorter bay the peak at $k_1 l_1 = 1.4$ is due to the influence of the fundamental mode of the first bay at that frequency. The small peak at $k_1 l_1 = 4.3$ also appears in the shorter bay, corresponding to the first resonant mode of the first (longer) bay. These results coincide with the linear solution shown by *Liu et al.* [2004].

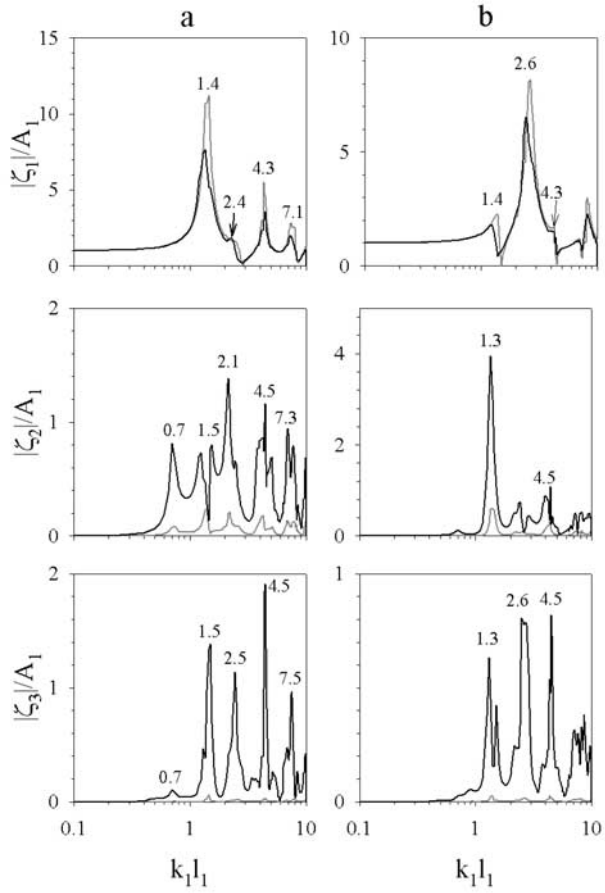

Figure 7. Response curves of the first three harmonics in (a) the first (longer) bay and (b) the second (shorter) bay for a dimensionless distance between the bays $d = 0.1\ l_1$. Shaded lines are the results for the almost linear case ($\varepsilon = 0.01$), and black lines are for the nonlinear case ($\varepsilon = 0.1$). Main peaks are labeled in terms of $k_1 l_1$.

[32] Comparing the nonlinear responses for the longer bay in the coupled system with those for a single bay (Figure 6) shows similar patterns of resonance peaks in all three harmonics. However, because of coupling, an additional peak for the first harmonic appears at $k_1 l_1 \sim 2.4$, which corresponds to the fundamental mode of the shorter (second) bay. Furthermore, for the second harmonic the relative importance of resonant peaks changes. For instance, the response peak of the second harmonic at $k_1 l_1 \sim 2.1$ for the

longer bay of the coupled system (Figure 7a (middle)) is bigger than that in the single bay case (Figure 6b). Similarly, the response peak of the second harmonic at $k_1l_1 \sim 1.3$ (or $k_1l_1 \sim 0.7$) in the shorter (longer) bay increases from 0.85 in the single bay system (corresponding to $k_1l = 0.7$ in Figure 6b) to more than 4 in the coupled system (Figure 7b (middle)). These phenomena can be explained as follows. At $k_1l_1 \sim 1.3$ the wave system is resonated in the longer bay. The corresponding wave frequency of the second harmonic is roughly $k_1l_1 \sim 2.6$, which is also very close to the fundamental mode of the shorter bay $k_1l_2 = 1.3$, resulting in the large increase in the second harmonic response in the shorter bay. Likewise, at $k_1l_1 \sim 2.4$ (or $k_1l_2 = 4.8$) the second bay is resonated and the corresponding second harmonic has the wave frequency at $k_1l_1 \sim 4.8$, which is very close to the first resonant mode of the longer bay. Therefore the second harmonic of the incident wave at $k_1l_1 \sim 2.1$ is resonated in the longer bay, yielding a relatively high response. Finally, the large response of the third harmonic in the shorter bay at incident frequency $k_1l_1 = 2.6$ is because the corresponding third harmonic frequency is roughly $k_1l_1 = 7.2$, which is very close to the second resonate frequency of the bay.

[33] In order to compare the results of the present analytical model with the field data, the amplifications calculated from the present analytical solutions in terms of the oscillation frequency inside the inlets under an almost linear condition, with $\varepsilon = 0.01$, and a nonlinear condition, with $\varepsilon = 0.1$, are shown in Figure 8. The total amplification is calculated as the sum of the contribution of all three harmonics that have the same frequency. Therefore, to convert the response curves to the total amplification at a particular frequency, say σ, one needs to add up the values of the response for the nth harmonic at a frequency $n\sigma$. Amplification peaks have been labeled with the corresponding periods in physical dimensions for a better comparison with field data. Nonlinear effects produce a clear reduction of the fundamental resonant mode in inlet 1 (period T = 10 min). This reduction appears for a single inlet as well and is not due to the coupling. In inlet 2, however, the behavior is opposite, the nonlinear solution is slightly larger than the linear one at the fundamental mode (T = 5 min). This increase is clearly related to the presence of the adjacent inlet and is the major manifestation of nonlinear coupling. As previously showed (Figure 7) this effect is primarily due to the contribution of the second harmonic. The same behavior is also observed in the field data (Figure 2), especially in the rissaga case, although the increase of the resonant peak for the nonlinear case is much more evident in the field observations.

[34] Other facts revealed in the field data are also present in the analytical solutions. For example, the energy content of the higher-order modes of Ciutadella (T = 4.1 min, 2.4 min) increases during rissaga (Figure 2a). Similar increases are also observed in the analytical solutions at T = 3.3 min and 1.9 min as shown in Figure 8a. Observations show an increase of energy during rissaga of the resonant responses due to the coupling, located at T $\sim$ 6 min for the first inlet (Ciutadella) and T $\sim$ 4 min for the second inlet (Platja Gran). The same effect is present in the analytical solutions (Figure 8). Finally, the peak that appears in inlet 2 because of the coupling with the fundamental mode of inlet 1, which is at 10.2 min, decreases with nonlinearity in both the analytical solutions and observations. The latest is a consequence of the smaller energy content in the fundamental mode of inlet 1 under nonlinear conditions.

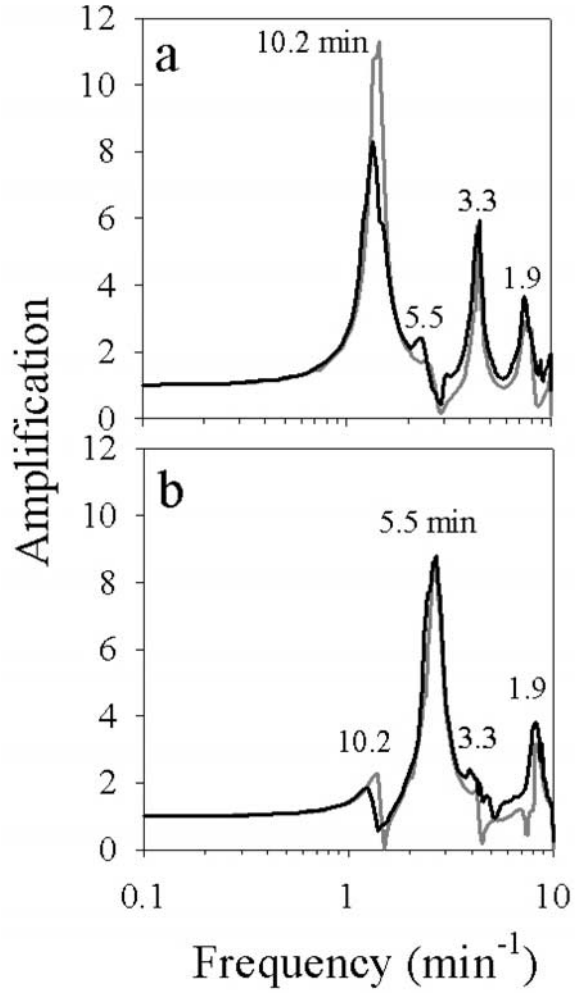

Figure 8. Amplifications computed for (a) inlet 1 and (b) inlet 2 under almost linear ($\varepsilon = 0.01$) (shaded lines) and fully nonlinear conditions ($\varepsilon = 0.1$) (black lines). Peaks are labeled with their periods in minutes.

6. Concluding Remarks

[35] A field experiment in Ciutadella region provides evidence on the resonance coupling between two bays during periods with different forcing conditions. An analytical model has been developed in order to explain the coupling effects and the different behaviors under linear and nonlinear wave conditions. On the basis of the Boussinesq equations we have studied theoretically the nonlinear coupling of two adjacent narrow, rectangular bays. Detailed analysis is presented for the case where the ratio of bay lengths is exactly two. This particular length ratio sets up a rather complex resonance coupling.

[36] Computed responses inside the bays reproduce the observed resonant modes. In addition to the modes of each inlet, the natural resonant modes of the adjacent inlet are also present in each bay, because of the coupling. When

nonlinearity is important the coupling mechanism becomes more complex and the relative amplification of the responses at different frequencies changes. The responses of both bays during a period with high activity are well reproduced by the model.

[37] The fact that analytical solutions demonstrate that the greater amplification of the fundamental mode of Platja Gran during a rissaga event can be explained as a nonlinear coupling has important implications. During rissaga events the amplifications are actually smaller than those predicted by linear theory at Ciutadella, but are considerably larger at Platja Gran. The generally accepted perception that nonlinearity may reduce the expected oscillations may be incorrect under specific circumstances. Any attempt to simulate the phenomenon to investigate the possible influence of any planned actuations in the inlets, should therefore consider not only the nonlinearity but also the presence of the adjacent inlet.

[38] The results presented in this paper can be used as a benchmark problem to verify more sophisticated transient numerical models based on either Boussinesq equations or shallow water equations. A laboratory experiment is also being planned to explore the problem further. Dissipative mechanisms such as entrance loss and bottom friction will be then considered in the formulation.

[39] **Acknowledgments.** The research reported here was initiated when the senior author (P. L.-F. Liu) was visiting IMEDEA as a "Profesor Visitante Iberdrola de Ciencia y Tecnología". The research was also supported by National Science Foundation grants to Cornell University (BES-9714182, CMS-9908392). The senior author would like to thank Cliff Astill, director of Geo-Hazard program at the National Science Foundation, for his continuous support. CICYT-CYTMAR MAR95-1863 project provided the necessary funding for the acquisition of the data. The authors would like to thank R. Medina, I. Losada, C. Vidal and F. Martín from the Ocean and Coastal Research Group at the University of Cantabria for their collaboration on the design and developing of LAST-97 measurements in Ciutadella region.

References

Emery, W. J., and R. E. Thomson (1997), *Data Analysis Methods in Physical Oceanography*, 634 pp., Pergamon, New York.

Gomis, D., S. Monserrat, and J. Tintoré (1993), Pressure-forced seiches of large amplitude in inlets of the Balearic Islands, *J. Geophys. Res.*, *98*, 14,437–14,445.

Liu, P. L.-F., S. Monserrat, M. Marcos, and A. B. Rabinovich (2003), Coupling between two inlets: Observation and modeling, *J. Geophys. Res.*, *108*(C3), 3069, doi:10.1029/2002JC001478.

Liu, P. L.-F., S. Monserrat, M. Marcos, and A. B. Rabinovich (2004), Correction to "Coupling between two inlets: Observation and modeling," *J. Geophys. Res.*, *109*, C03011, doi:10.1029/2003JC002016.

Mei, C. C. (1989), *The Applied Dynamics of Ocean Surface Waves*, 740 pp., World Sci., River Edge, N. J.

Miles, J. W. (1994), Harbor seiching, *Annu. Rev. Fluid Mech.*, *6*, 17–35.

Monserrat, S., A. Ibbetson, and A. J. Thorpe (1991), Atmospheric gravity waves and the 'rissaga' phenomenon, *Q. J. R. Meteorol. Soc.*, *117*, 553–570.

Monserrat, S., A. B. Rabinovich, and B. Casas (1998), On the reconstruction of the transfer function for atmospherically generated seiches, *Geophys. Res. Lett.*, *25*, 2197–2200.

Nwogu, O. (1993), An alternative form of the Boussinesq equations for nearshore wave propagation, *J. Waterw. Port Coastal Ocean Eng.*, *119*, 618–638.

Panchang, V., and Z. Demirbilek (2001), Simulation of waves in harbors using two-dimensional elliptic equation models, in *Advances in Coastal and Ocean Engineering*, vol. 7, edited by P. L.-F. Liu, pp. 125–162, World Sci., River Edge, N. J.

Press, W. H., B. P. Flannery, S. A. Teukolsky, and W. T. Vetterling (1989), *Numerical Recipes*, Cambridge Univ. Press, New York.

Rabinovich, A. B., and S. Monserrat (1998), Generation of meteorological tsunamis (large amplitude seiches) near the Balearic and Kuril Islands, *Nat. Hazards*, *18*, 27–55.

Rogers, S. R., and C. C. Mei (1978), Nonlinear resonant excitation of a long and narrow bay, *J. Fluid. Mech.*, *88*, 161–180.

Tintoré, J., D. Gomis, S. Alonso, and D. P. Wang (1988), A theoretical study of large sea level oscillations in the western Mediterranean, *J. Geophys. Res.*, *93*, 10,797–10,803.

Woo, S.-B., and P. L.-F. Liu (2004a), A finite element model for modified Boussinesq equations. Part I: Model development, *J. Waterw. Port Coastal Ocean Eng.*, *130*, 1–16.

Woo, S.-B., and P. L.-F. Liu (2004b), A finite element model for modified Boussinesq equations. Part II: Applications to nonlinear harbor oscillations, *J. Waterw. Port Coastal Ocean Eng.*, *130*, 17–28.

P. L.-F. Liu, School of Civil and Environmental Engineering, Cornell University, 105 Hollister Hall, Ithaca, NY 14853, USA.

M. Marcos and S. Monserrat, Grup d'Oceanografia Interdisciplinar/Oceanografia Física (GOIFis), IMEDEA (CSIC-UIB), 07190 Esporles, Mallorca, Illes Balears, Spain. (s.monserrat@uib.es)